Characterization of the composition, structure, and seasonal variation of the mixing layer above the extratropical tropopause as revealed by MOZAIC measurements

Jérôme Brioude, Jean-Pierre Cammas, O. R. Cooper, P. Nedelec

Characterization of the composition, structure, and seasonal variation of the mixing layer above the extratropical tropopause as revealed by MOZAIC measurements

J. Brioude,[1,2] J.-P. Cammas,[3] O. R. Cooper,[1,2] and P. Nedelec[3]

Received 18 July 2007; revised 4 March 2008; accepted 28 March 2008; published 15 July 2008.

[1] The chemical composition of the mixing layer above the tropopause, which is mainly influenced by stratosphere troposphere exchange, impacts the chemistry and radiative balance of the troposphere. A better understanding of its seasonal and spatial variation is needed to reduce uncertainties of global chemistry-transport models. In this paper, we use the Measurements of Ozone, Water Vapour, Nitrogen Oxides and Carbon Monoxide by Airbus In-Service Aircraft (MOZAIC) ozone and carbon monoxide data from 2003. The five MOZAIC aircraft fly daily between Europe and North America and between Europe and Asia, at 9–12 km crossing the tropopause when transecting upper level troughs. We present a new coordinate system consisting of potential vorticity on the *y* axis and the angle between the local PV surface and the horizontal on the *x* axis to study the mixing that occurs in the tropopause region. This coordinate system allows us to view the typical distribution of ozone and CO within upper level troughs. Using in situ measurements and a Lagrangian analysis, we have identified a mixing layer associated with stirring and mixing in the tropopause region between 2 and 6 pvu. Regional variations of the ozone and CO distributions and chemical anomalies between the center and the borders of the upper level troughs are found within the mixing layer.

Citation: Brioude, J., J.-P. Cammas, O. R. Cooper, and P. Nedelec (2008), Characterization of the composition, structure, and seasonal variation of the mixing layer above the extratropical tropopause as revealed by MOZAIC measurements, *J. Geophys. Res.*, *113*, D00B01, doi:10.1029/2007JD009184.

1. Introduction

[2] The upper troposphere and lowermost stratosphere (UTLS) is a key region of the atmosphere because it is the mixing zone between tropospheric and stratospheric air masses which impacts the chemistry and radiative forcing of the atmosphere. In the UTLS at midlatitudes, a net mass flux exists from the stratosphere to the troposphere [*Appenzeller et al.*, 1996]. The Brewer-Dobson circulation controls the downward flux from the middle stratosphere to the lowermost stratosphere, below the 380 K isentropic surface. Then, processes such as stratospheric intrusions, cutoff lows and gravity waves allow ozone to enter the troposphere [*Stohl et al.*, 2003].

[3] As a consequence, a change of the ozone concentration in this region changes the stratospheric flux of ozone into the troposphere and then impacts tropospheric chemistry. Furthermore, variations of ozone concentration in the UTLS lead to radiative flux variations at the surface, and perturbs the surface temperature [*Forster and Shine*, 1997].

[4] Stratosphere troposphere exchange (STE) is composed of stratosphere to troposphere transport (STT) and troposphere to stratosphere transport (TST). In midlatitudes, the cross tropopause flux associated with STT is greater than TST. An accurate knowledge of these transport processes is of great importance in quantifying the relative roles of transport and chemistry in the budgets of trace gases as diagnosed by global chemistry-transport models (CTM), the tools used to quantify the tropospheric ozone budget and to provide information to policy makers and industry. Large differences in the stratospheric source, from 400 $Tg(O_3)\ a^{-1}$ [*Hauglustaine et al.*, 1998] to 1000 $Tg(O_3)\ a^{-1}$ [*Crutzen et al.*, 1999], were apparently responsible for wether or not a model calculated a chemical source or sink of tropospheric O_3 [*Intergovernmental Panel on Climate Change*, 2001]. Recent studies [*Stevenson et al.*, 2006; *Grewe*, 2006] have shown that the CTMs converge to a lower uncertainty of stratospheric ozone flux, between 420 and 520 $Tg(O_3)\ a^{-1}$, with intermodel standard deviations of 38%. All these models predict a net photochemical production of ozone in the troposphere.

[5] STE is mainly due to mixing occurring on isentropic surfaces near breaking Rossby waves and by stirring effects

[1] Chemical Sciences Division, Earth System Research Laboratory, NOAA, Boulder, Colorado, USA.
[2] Also at Cooperative Institute for Research in Environmental Sciences, University of Colorado, Boulder, Colorado, USA.
[3] Laboratoire d'Aérologie, UMR5560, CNRS, Observatoire Midi-Pyrénées, Toulouse, France.

0148-0227/08/2007JD009184

due to differential advection near the jet stream. Previous case studies [e.g., *Hoor et al.*, 2002; *Pan et al.*, 2004] have used ozone and CO relationships to characterize mixing processes in the tropopause region. They have shown that transport across the extratropical tropopause produces a mixed layer with linear relationships between ozone and CO, in cases of recent mixing events. Trace gas isopleths in this mixing layer follow the shape of potential vorticity surfaces (PV [*Krebsbach et al.*, 2006]).

[6] Tracer analyses in the stratosphere are usually based on a meridional coordinate system because the tropopause slopes downward and poleward, intersecting isentropic surfaces at midlatitudes. These analyses use areas encompassed by PV contours (equivalent latitude) or with tracer contours (tracer equivalent latitude [*Allen and Nakamura*, 2003]). These coordinates are used to study processes within the polar vortex, initialization of models, and isentropic tracer exchange across the tropopause [e.g., *Manney et al.*, 1999; *Lary et al.*, 1995; *Seo and Bowman*, 2001; *Hoor et al.*, 2004; *Hegglin et al.*, 2006]. Using these meridional coordinate systems, these studies do not address the variation of STE fluxes that occurs along a line of constant latitude. However, the tropopause also intersects the isentropes zonally in baroclinic waves. In upper level troughs, the isentropes intersect the dynamic tropopause near the jet stream where the tropopause is tilted. *Sprenger and Wernli* [2003] have shown that STE processes vary zonally and seasonally. They occur frequently in the storm track regions near the east coasts of North America and Asia. Thus, to accurately study the zonal and seasonal variations of STE processes, it is necessary to study in detail the STE processes at synoptic scales in baroclinic waves.

[7] In this paper, we use in situ measurements of ozone and CO from the Measurements of Ozone, Water Vapour, Nitrogen Oxides and Carbon Monoxide by Airbus In-Service Aircraft (MOZAIC) program [*Marenco et al.*, 1998; *Thouret et al.*, 1998b] (http://mozaic.aero.obs-mip.fr) to improve our knowledge of STE processes in midlatitudes.

[8] The MOZAIC aircraft fly at altitudes between 9 and 12 km and most of the time cross the tropopause when they encounter upper level troughs which have lower tropopause heights than upper level ridges. The MOZAIC program has an extensive spatial coverage spanning from Europe to the west coast of North America, and from Europe eastward to the east coast of Asia. Flying once or twice per day, the five aircraft also provide good temporal coverage. A climatological analysis of the UTLS region with MOZAIC data requires a coordinate system in which the dynamic characteristics of upper level troughs can by synthesized.

[9] We present in this article a new coordinate system to report in situ measurements from the MOZAIC database within the context of a composite upper level trough. The coordinate system is based on PV on the y axis, and on the angle between the local tropopause and the horizontal along latitude circles in the zonal direction on the x axis. We focus on upper level troughs because the MOZAIC flights are limited to altitudes below 12 km and therefore have a more extensive depth of sampling of the lower stratosphere above upper level troughs rather than above upper level ridges.

[10] We use 1 year of MOZAIC measurements to (1) reveal the distribution of ozone and CO within the upper level troughs, (2) identify a mixing layer within the lower stratosphere above upper level troughs, and (3) highlight the zonal and seasonal variations of STE within the troughs.

2. Method

2.1. Dynamic Coordinate System

[11] The MOZAIC program provides on board measurements of ozone, CO, NOy and water vapor from commercial aircraft. MOZAIC was funded to have comprehensive and continuous observations, for the purpose of assessing climate change. The five MOZAIC aircraft fly almost daily and provide a high horizontal resolution of about 1 km. On the basis of the dual-beam UV absorption principle, the ozone measurement accuracy is estimated at ±2 ppbv ±2% [*Thouret et al.*, 1998a] for a 4s response time. On the basis of an infrared analyzer, the carbon monoxide measurement accuracy is estimated at ±5 ppbv ±5% [*Nédélec et al.*, 2003] for a 30 s response time. In this study, we use the MOZAIC data at midlatitudes ($\geq$20°). We also define the extratropical tropopause as the 2 pvu surface.

[12] Upper troughs are known to be regions where STT (predominantly through tropopause folds) and TST (predominantly through WCB) occur frequently, the magnitude of the transport depending on the baroclinic life cycle [*Polvani and Esler*, 2007]. In upper troughs, the tropopause intersects the pressure and isentropic surfaces. This fact prevents the use of pressure or potential temperature to define the tropopause or to evaluate the position of a measurement in the lowermost stratosphere relative to the local tropopause. Furthermore the tropopause intersects different isentropic surfaces depending on the magnitude of the PV anomaly [*Hoskins et al.*, 1985], the latitude or the season. Therefore we use PV in this paper to define the tropopause. In addition, the mixing layer between troposphere and stratosphere follows PV surfaces rather than isentropic surfaces [*Hoor et al.*, 2004; *Krebsbach et al.*, 2006]. Hence PV can also be used as a coordinate to indicate the position of an in situ measurement within the mixing layer and the lowermost stratosphere. PV in this study is calculated from gridded model output at much coarser resolution that the 1 km MOZAIC measurements and uncertainties may arise from the interpretation of fine scale in situ measurements with modeled parameters.

[13] Figure 1a presents the potential temperature (θ) and PV surfaces in a zonal cross section (10–60°E) at 55°N. An upper level trough with two lobes is at the center of the cross section. In this PV anomaly, the PV surfaces are deformed by dynamic processes such as Rossby waves on the synoptic scale or upper level frontogenesis on the mesoscale.

[14] The principle of our dynamic coordinate system is to use the angle α calculated between the local PV surface and the horizontal in the zonal direction to specify if an observation has been measured on the east side, the west side or the center of a trough. We also use PV as a parameter for evaluating the depth of the observations within the lowermost stratosphere relative to the local tropopause. By convention, when cross cutting from east to west, α is positive when the horizontal PV gradient is negative (the right side of Figure 1) and negative when the horizontal PV gradient is positive (the left side of Figure 1). The three-

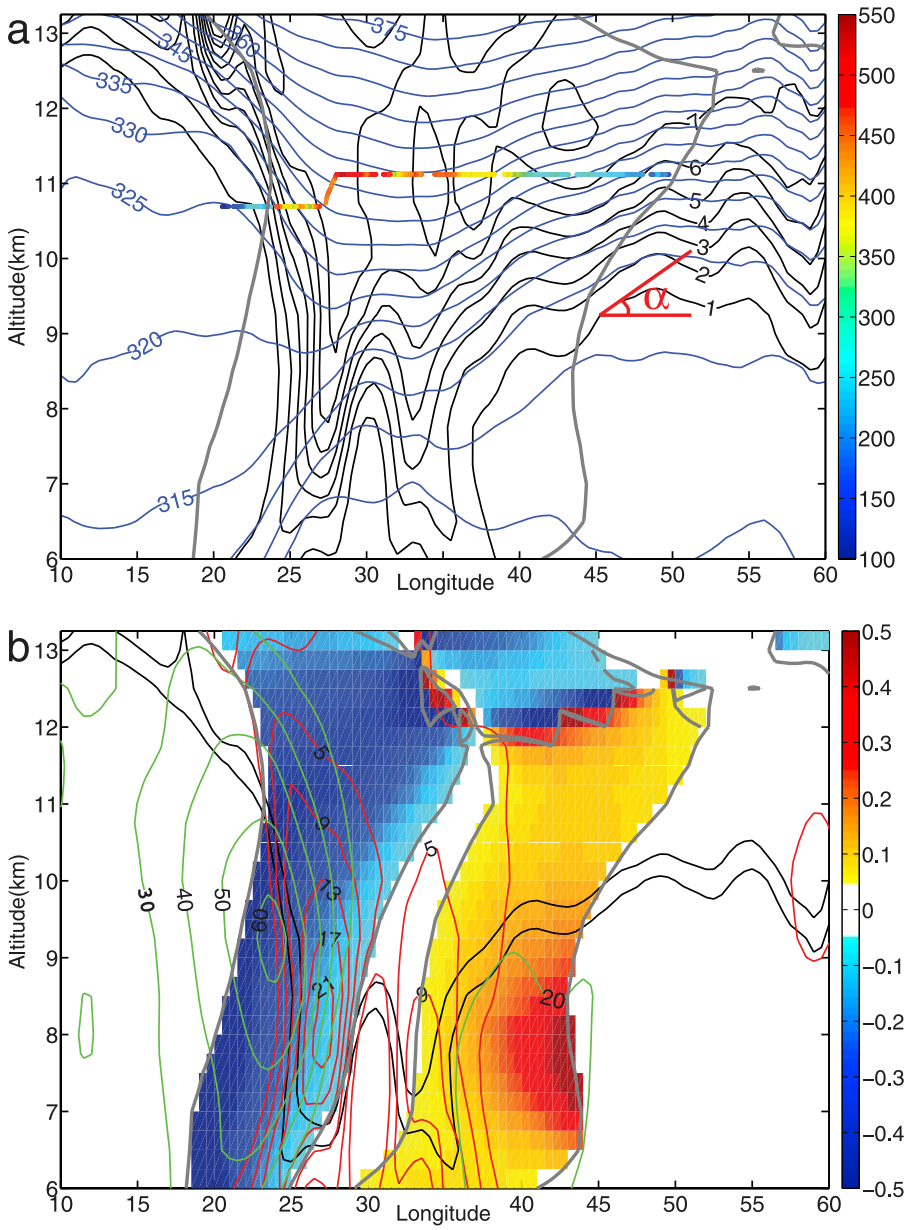

Figure 1. (a) PV surfaces (black contours, from 1 to 7 pvu) and potential temperature surfaces (blue contours, from 300 to 370 K) and (b) wind speed (green contours, from 20 to 60 m s^{-1}), relative vorticity (red contours, from 1 to 21 10^{-5} s^{-1}), and angle α of PV surfaces with the horizontal after filtering the PV fields (color code, from −0.5 to 0.5) in a zonal vertical cross section at 55°N latitude. The outer grey lines represent the position where the second derivative of the filtered PV surfaces is zero in the cross section, while the inner grey lines (Figure 1b) represent the position of the center of the trough, defined by $|\alpha| \geq 0.5$. The area encompassed by the grey lines represents the region of the upper level trough. In Figure 1a, the aircraft pathway of the MOZAIC flight on 9 March 2003 at about 2100 UTC in the upper level trough region is colored by the ozone mixing ratio (colored dots, ppbv).

dimensional PV fields are retrieved using model-level data from the European Centre for Medium-Range Weather Forecasts (ECMWF) with a temporal resolution of 3 h (analyses at 0000, 0600, 1200, and 1800 UTC; forecasts at 0300, 0900, 1500, and 2100 UTC), with a horizontal resolution of 0.5° × 0.5°, and 60 vertical levels. Thus, the PV values in the next sections are calculated with a horizontal resolution of 0.5°.

[15] At 0.5° of resolution, positive or negative α values lie respectively on both sides of the upper level trough because of the lobes caused by upper level frontogenesis and mesoscale PV features. Thus a coordinate (α_o, PV_o) may be related to positions on both sides of the upper level trough, and cannot be considered as a frame of reference. A low-pass filter is applied in the Fourier domain to retain PV zonal wavelengths longer than 25° in longitude while

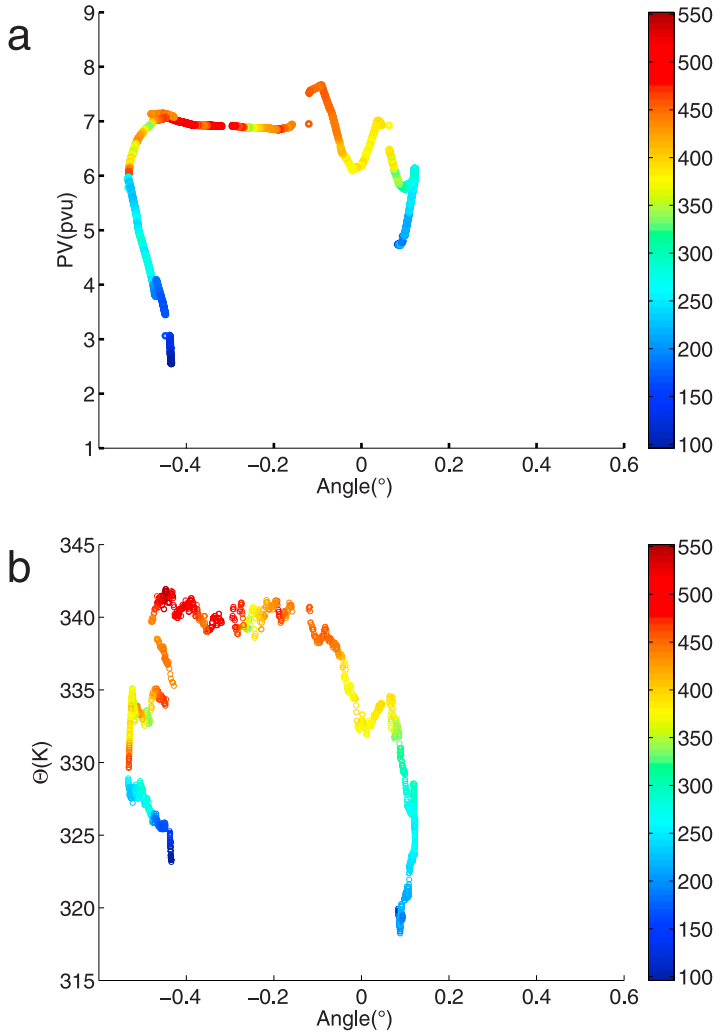

Figure 2. MOZAIC ozone measurements from Figure 1, shown in cross section 1 with α on the x axis and (a) PV (pvu) and (b) potential temperature (K) on the y axis.

discarding mesoscale features. The choice of 25° is a compromise between the fact that the threshold is large enough to filter the mesoscale PV features, and small enough to calculate α within a realistic upper trough. Threshold values of 18° and 32° were also used but the results were similar to those obtained with 25°. Then, using the filtered PV field, α values are based on the zonal PV gradient calculated over a length of 5°, and the vertical PV gradient calculated over three model levels (about 1.5 km in depth near the extratropical tropopause). The α values are not sensitive to this length. As a consequence, using the filtered PV surfaces, α values in Figure 1b are positive on the east side (red color) and negative on the west side (blue color) and close to zero along the axis of the upper level trough (white color).

[16] Above 8 or 9 pvu (above 12 km of altitude), the vertical PV gradient is sometimes zero or negative, increasing the α variability. However, as the maximum altitude of MOZAIC aircraft is 12 km and the minimum altitude of the extratropical tropopause is 6 km, the MOZAIC aircraft fly at relatively low altitudes in strong PV anomalies most of the time in a positive vertical gradient for PV values greater than 8 pvu. Thus, PV can still be used as a vertical coordinate when values are greater than 8 pvu. To select the MOZAIC data in upper level troughs, we retain only the positive values of the second derivative of PV (Figure 1a, between the two grey lines), calculated over a length of 40° of longitude. Negative values, related to upper level ridges are discarded. The results in the following sections are not sensitive to this length.

[17] The MOZAIC flight track on 9 March 2003 around 2100 UTC, colored by the ozone mixing ratio, is shown in Figure 1a. The aircraft crossed the upper level trough from west to east. The aircraft pathway is represented in an (α_o, PV_o) coordinate system in Figure 2a and in an (α_o, Θ_o) coordinate system in Figure 2b. It shows that the aircraft has entered the upper level trough in a steep α region ($\alpha \leq -0.4$) on the west side and then flew between 5 and 7 pvu across the upper level trough. The α values are small, with an absolute value less than 0.6°, because the horizontal scale of the PV features is a few hundred kilometers while the vertical scale is just a few kilometers. Notice that the average ozone mixing ratio at the center of the upper level trough ($-0.05 \leq \alpha \leq 0.05$, 6 pvu $\leq$ PV $\leq$ 7 pvu, $\Theta \simeq 335$ K) is

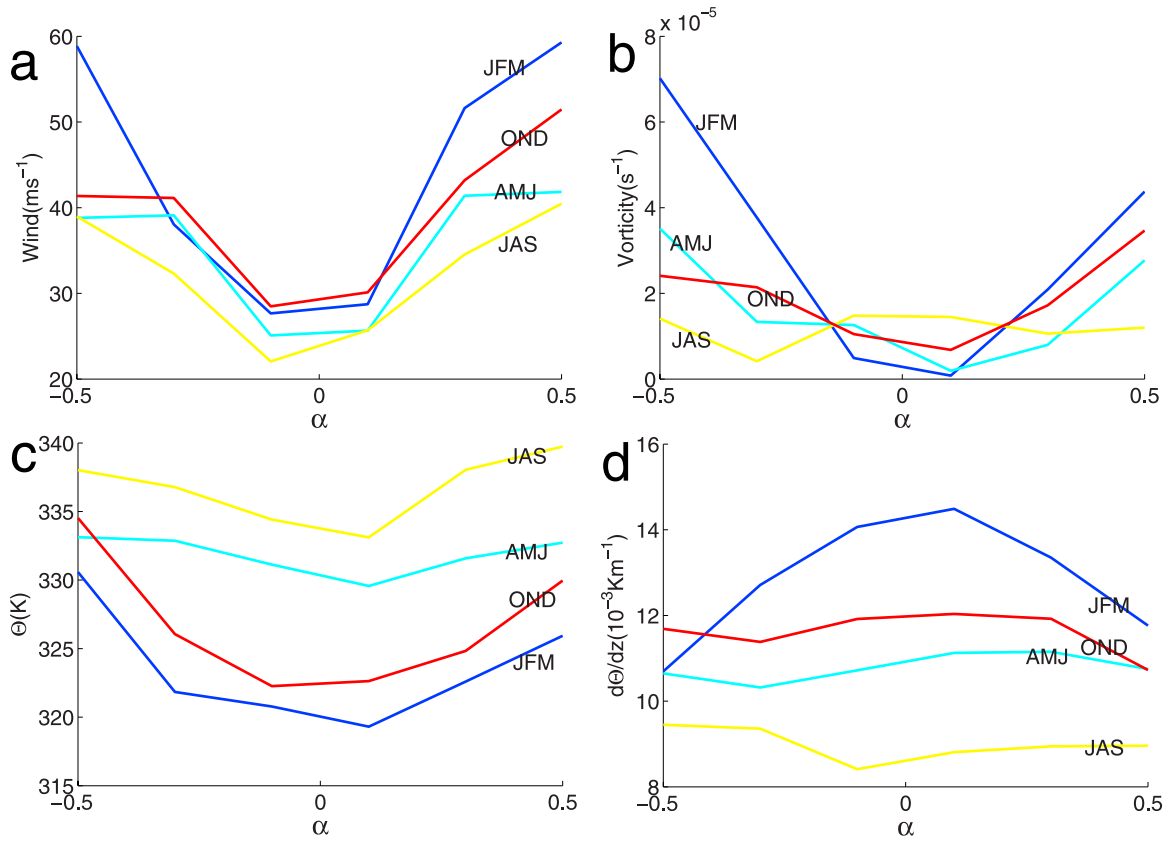

Figure 3. Mean values of (a) wind speed (m s^{-1}), (b) vorticity (s^{-1}), (c) potential temperature (K), and (d) vertical gradient of potential temperature (10^{-3} K m^{-1}) averaged over PV ranging between 2 and 4 pvu and for α angles ranging between -0.6 and 0.6 in January–February–March (JFM), April–May–June (AMJ), July–August–September (JAS), and October–November–December (OND).

less than at the western border ($\alpha \leq -0.2$). This negative anomaly of ozone in the upper level trough is studied in detail at the seasonal timescale in section 3.1 and in section 5 with hundreds of MOZAIC flights. Commercial aircraft follow a northward curve across midlatitudes because they follow great circle routes between continents. Thus, the MOZAIC aircraft most often cross the tropopause at the northern extent of upper level troughs, where they are zonally wider than at more southerly latitudes. By selecting only the wide upper level troughs, we constrained the MOZAIC data to be located in the northern part of upper level troughs. Furthermore, along a latitude circle, an aircraft crossing a wide upper level trough will spend more time at low zonal angle α (the center) than large zonal angles α (the borders). As a consequence, the number of MOZAIC observations plotted in a (α_o, PV$_o$) coordinate system are biased toward low zonal angles.

2.2. Validation

[18] In this section, we first describe the variations of potential temperature, relative vorticity and wind speed with respect to the angle α along a layer near the tropopause within the upper trough of Figure 1. Then, in order to validate the method, we compare these variations to the seasonal-scale variation shown on Figure 3.

[19] On Figure 1b, the relative vorticity is calculated with a resolution of 1° using the ECMWF wind fields. On a given PV surface in Figure 1b, the shorter the distance to the core of the jet stream, the steeper the angle α between the horizontal and the local PV surface. At the center of the anomaly, α is zero with a local wind speed minimum. Then, on a PV surface, the smallest θ values lie at the center of the positive PV anomaly, while the greatest θ values lie on the borders. Furthermore, on a given PV surface, the curvature component of the relative vorticity is positive everywhere and the shear component of the relative vorticity is positive and at a maximum on the cyclonic shear side of the jet stream [*Bell and Keyser*, 1993]. Thus, on a given PV surface, the relative vorticity is positive everywhere and at a maximum on the borders of the trough.

[20] To validate the method on the seasonal scale, we use the MOZAIC measurements of potential temperature and wind speed. In addition, we use the relative vorticity and the vertical gradient of potential temperature ($d\theta/dz$, representing the local static stability) calculated from the ECMWF fields. The variations of these parameters are studied with respect to α and averaged over PV values ranging from 2 to 4 pvu. To obtain the values of α, PV, relative vorticity and $d\theta/dz$ at each MOZAIC data point, we interpolate the diagnostic fields linearly in space and time using the two nearest ECMWF fields. This method assumes that advection of PV features varies linearly in space and time.

[21] Figure 3 presents the average wind speed (Figure 3a), relative vorticity (Figure 3b), the potential temperature

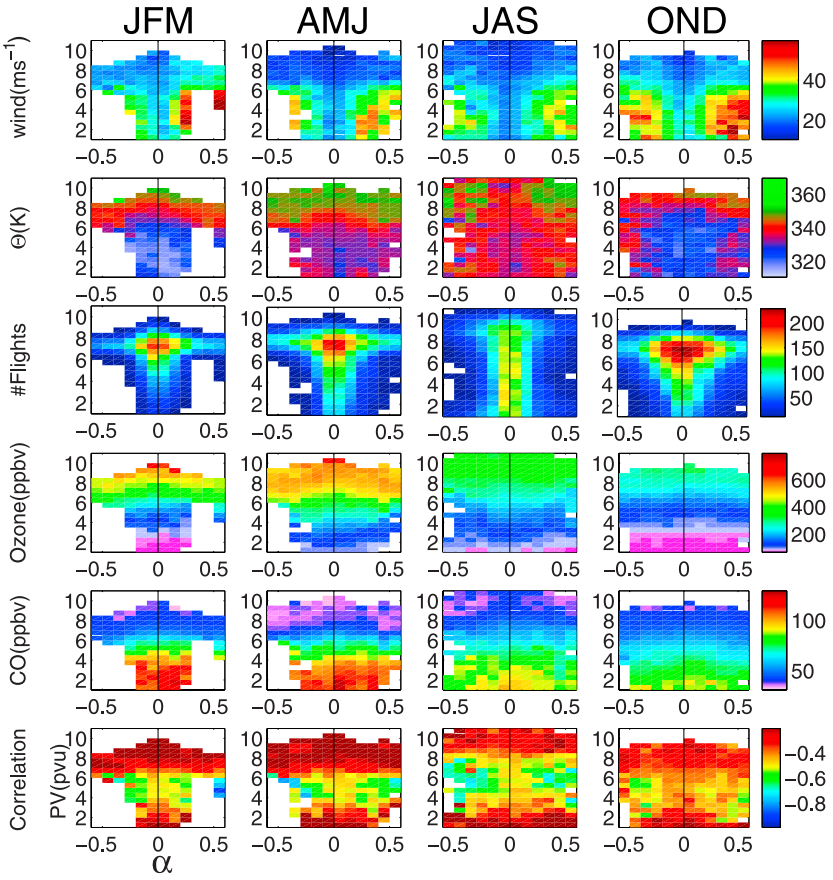

Figure 4. MOZAIC wind speed (m s^{-1}) (first row), potential temperature (K) (second row), number of MOZAIC flights (third row), ozone mixing ratio (ppbv) (fourth row), CO mixing ratio (ppbv) (fifth row), and ozone/CO correlation in the dynamic coordinate system (α, PV) (sixth row) associated with MOZAIC flights between JFM (first column), AMJ (second column), JAS (third column), and OND (fourth column) in 2003. The data are plotted in a coordinate system with the angle of the local PV surface α on the x axis and the PV value on the y axis.

(Figure 3c) and $d\theta/dz$ between 2 and 4 pvu (Figure 3d), for the four seasons in 2003. These plots represent the variations of these parameters near the tropopause within the composite upper trough at the seasonal scale. The wind speed, relative vorticity and potential temperature are highest at the borders, and smallest at low α, while $d\theta/dz$ is smallest at the borders and highest at the center. The greatest MOZAIC wind speeds are associated with the largest α values, confirming that the angle of a PV surface is related to the wind speed, and the cores of the upper jet streams are associated with the largest α. The relative vorticity is positive, and the greatest vorticity is associated with the largest α values, near the cyclonic shear side of the upper jet streams. The behavior of $d\theta/dz$ is the opposite of the relative vorticity behavior which is expected on a PV surface as the static stability must be reduced near the cyclonic shear side to compensate for the increase of relative vorticity to have the PV conserved. The greatest MOZAIC potential temperature values are associated with the largest α values. On a given PV surface, the center of the trough is associated with lower potential temperature than the borders, confirming that the PV surfaces are located at a lower altitude at low α, and at higher altitude at large α.

[22] By comparing the behavior of these 4 dynamic parameters in the (α_o, PV$_o$) coordinate system described above with the zonal cross section of the upper trough (Figure 3), we show that the dynamic coordinate system provides a coherent picture of the MOZAIC measurements within a composite upper level trough. The lowest values of wind speed, relative vorticity and the greatest values of potential temperature are found during summer, while the greatest values of wind speed and vorticity and the lowest values of potential temperature are found in winter.

[23] The fact that the strongest relative vorticity is found on the edges at the seasonal scale shows that the MOZAIC aircraft fly more frequently in asymmetric PV anomalies because of the position of jet streaks upstream or downstream of the upper troughs. At the cutoff low stage, which is not discarded by our method, the cyclonically curved jet makes the shear component and curvature component overlap, with a maximum of relative vorticity along the axis of the trough [*Bell and Keyser*, 1993].

[24] Figure 4 presents MOZAIC wind speed (first row), θ (second row), and the number of MOZAIC flights in each 0.1° and 1 pvu (α_o, PV$_o$) grid cell (third row), for four time periods in 2003: January–February–March (JFM, 264 flights)

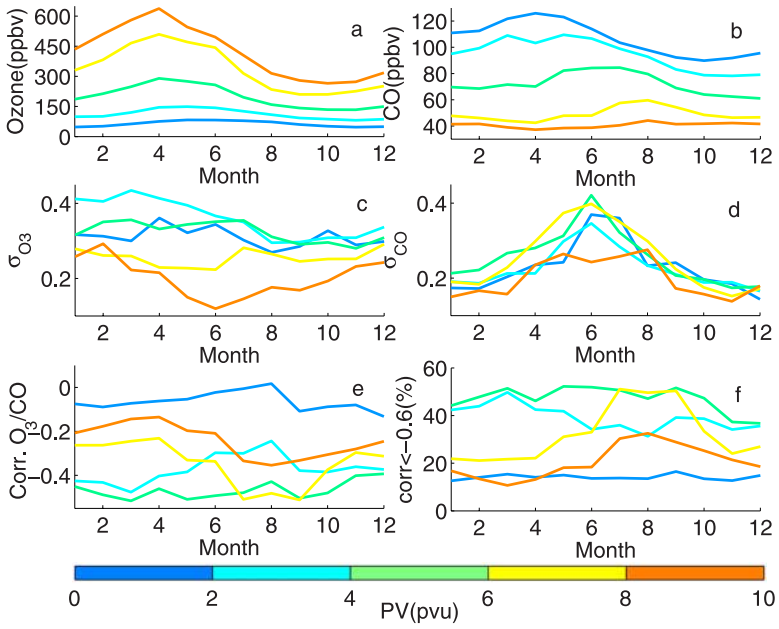

Figure 5. Mean (a) ozone(ppbv) and (b) CO(ppbv) for each month (abscissa), calculated for each 2 pvu interval from 0 to 12 pvu. Normalized standard deviation of (c) ozone and (d) CO. (e) Mean ozone/CO correlation for each month. (f) Percentage of observations with an ozone/CO correlation less than −0.6.

defined as winter, April–May–June (AMJ, 365 flights) defined as spring, July–August–September (JAS, 434 flights) defined as summer, October–November–December (OND, 512 flights) defined as fall. For each grid cell in the coordinate system (α_o, PV_o), a parameter is plotted if it is averaged using at least 10 different MOZAIC flights. Thus, each plotted parameter is the average of at least 10 different meteorological situations over a time period of 3 months. The number of empty grid cells diminishes with time from January–February to November–December as the frequency of MOZAIC CO observations increased during 2003.

[25] In Figure 4 the general distribution of data is narrow below the 6 pvu surface, and broader above the 6 pvu surface because of the smaller vertical gradient of PV that MOZAIC aircraft encounter above 6 pvu.

[26] On a given PV surface, the greatest MOZAIC wind speeds (greater than 40 m s^{-1}) are associated with the largest α values, confirming that the angle of a PV surface is related to the wind speed. For angle values near zero, the wind speed is low (between 10 and 20 m s^{-1}). This region is associated with the axis of upper level troughs.

[27] The distribution of MOZAIC flight frequency in the coordinate system (Figure 4, third row) shows a common aircraft pathway between 6 and 8 pvu in winter, spring and fall. In summer, the observations are homogeneous between 1 and 8 pvu. This is due to the seasonal variation of the tropopause height at midlatitudes linked to the average latitudinal position of the jet stream. The tropopause is lower in winter and spring and therefore the aircraft fly frequently above the tropopause. During summer, the tropopause height is higher and airliners cross the tropopause more frequently when they fly between upper level troughs and ridges.

[28] Furthermore, as discussed in the previous section, the aircraft fly often at the center of the upper level troughs, because of the great circle routes and also to avoid clear air turbulence.

[29] Ozone (fourth row) and CO (fifth row) averaged in (α, PV) grid cells for the four seasons in 2003 are presented in Figure 4. The seasonal cycles of ozone and CO and the existence of a mixing layer are discussed in section 3. Differences of ozone and CO between the center and borders of the composite upper level trough are discussed in section 5. Differences of ozone and CO between the east side and west side of the composite upper level trough are discussed in section 6.

3. Evidence for a Mixing Layer in the Tropopause Region

3.1. Ozone and CO Distributions

[30] In this section, we describe the seasonal cycle of ozone and CO and show the existence of a mixing layer in the tropopause region by investigating the spatial distribution of ozone and CO and ozone/CO correlations in the (α_o, PV_o) coordinate system.

[31] Figure 5 presents the average ozone (Figure 5a) and CO mixing ratio (Figure 5b) calculated for each 2 pvu interval from 0 to 10 pvu and for each month in 2003.

[32] Above the 6-pvu surface, the ozone mixing ratios show a seasonal cycle with a maximum in April at 640 ppbv and a minimum in October at 265 ppbv, in accordance with the Brewer Dobson circulation. For PV values less than 2 pvu, ozone mixing ratios show a seasonal cycle with a maximum in May and June at 83 ppbv, and a minimum in November to January at 47 ppbv, according to the seasonal cycle of the photochemical production of ozone in the troposphere. Between these two regions, the ozone seasonal variability is the product of these two cycles.

[33] Below the 2-pvu surface, the CO mixing ratios show a maximum in April and May of 125 ppbv and a minimum from September to November of 91 ppbv. This cycle is due to two different processes. (1) Vertical transport in the troposphere of CO emissions follows seasonal and zonal variations [*Stohl et al.*, 2002] with an increase of trace gas export from the boundary layer to the free troposphere from wintertime to springtime. (2) CO accumulates gradually in the troposphere from the end of the fall season to the beginning of spring because of reduced oxidation. Then, CO is rapidly oxidized by OH radicals between April and June [*Novelli et al.*, 1998]. This tropospheric cycle is visible up to 4 pvu. Because of the efficiency and frequency of STE near the tropopause, the tropospheric cycle of CO is predominant up to 4 pvu.

[34] Above 8 pvu, a stratospheric cycle of CO is also visible. A minimum of 37 ppbv occurs during April, with a maximum in August of 45 ppbv. This cycle may be explained by the fact that the lowermost stratosphere is more influenced by air descending from above 380 K during springtime than at the end of summer [*Ray et al.*, 1999]. It may also be due to the ''shorter pathway'' of the Brewer-Dobson circulation [*Rosenlof et al.*, 1997; *Hoor et al.*, 2005; *Hegglin et al.*, 2006]. Quasi-horizontal mixing along isentropic surfaces may rapidly transport air masses from the tropical tropopause to the lowermost stratosphere at midlatitudes [*Rosenlof et al.*, 1997]. Tropical convection may contribute to the chemical composition of the upper part of the lowermost stratosphere from 35% in spring to 55% in autumn [*Hoor et al.*, 2005]. Transport from the subtropics (with a CO background of about 55 ppbv) reduces the impact of the stratospheric contribution from above 380 K (with a CO background of about 15 ppbv) and thus increases the CO mixing ratios in the lowermost stratosphere [*Hoor et al.*, 2005].

3.2. Ozone and CO Relationship

[35] The stirring effect due to upper level jet stream dynamics can produce filaments such that sampling by aircraft along an isentropic surface over a distance of 50 km can cross successively different air masses of both tropospheric and stratospheric origin. Over 50 km, the stirring of filaments is the dominant process which homogenizes the chemical gradients. Diffusion dominates homogenization at a horizontal scale smaller than 20 km (e.g., 13 km in the work by *Haynes and Anglade* [1997]). In the case of measurements in the UTLS region, the horizontal branch in an ozone/CO scatterplot is related to the tropospheric reservoir and the vertical branch to the stratospheric reservoir [*Hoor et al.*, 2002]. Within a mixing region, recent mixing between these two reservoirs creates in an ozone/CO plot the so-called mixing lines, defined by a negative slope and thus a linear correlation coefficient close to -1. As time goes by, further diabatic and photochemical processes destroy this linear relationship between ozone and CO and the compactness of ozone/CO scatterplots, resulting in a reduction of the linear correlation between ozone and CO. The diabatic processes arise from radiative cooling and deep convection. As a consequence, looking at the ozone and CO relationship over 50 km, the linear correlation between ozone and CO can be used to indicate the existence of recent mixing governed by stirring between the troposphere and the stratosphere, with stronger anticorrelations related to more recent stirring and mixing.

[36] In this study we use measurements along 50 km flight segments to calculate the ozone/CO correlations, as a compromise between the fact that the segment length must be short enough to assume that each MOZAIC segment is located on an isentropic surface, and long enough to sample the linear relationship produced by stirring and mixing. However, the following results are insensitive to segment lengths which varied from 20 km to 100 km (not shown).

[37] In Figure 4 (sixth row), the strongest anticorrelations (≤ -0.6) are observed between 2 and 6 pvu, and particularly at the largest α values and strongest wind speed, near the edges of the upper jet streams. This region encompasses all isentropic surfaces crossing the upper level jet streams, which means that the stirring effect is likely the dominant process in this region compared to diabatic and small-scale diffusive processes. This region is related to the compact shape of ozone/CO scatter plots [*Hoor et al.*, 2002; *Pan et al.*, 2004] where mixing lines with negative slopes between the troposphere and the stratosphere are observed. The weakest anticorrelations are encountered under 2 pvu and above 6 pvu, and almost 8 pvu in July–August. Under 2 pvu the correlations are weakest probably because convective mixing in the troposphere destroys the chemical signature of mixing governed by stirring (up to 4 pvu in summertime). Above 6 pvu, the mixing governed by stirring is no longer dominant and photochemistry and diabatic processes influence the chemical distribution of ozone and CO. In July–August, the depth of the domain where mixing governed by stirring is dominant reaches 8 pvu, while the weakest anticorrelations are found below 4 pvu.

[38] Figure 5d shows the normalized standard deviation of CO (σ_{CO}) calculated for each interval of 2 pvu from 0 to 10 pvu. σ_{CO} is at a maximum in June between 0 and 8 pvu. For PV greater than 8 pvu, two relative maxima of σ_{CO} occur in May and August. In the troposphere (PV $\leq$ 2 pvu, dark blue), a maximum of variability is found in June, which may be due to deep convection penetrating into the lowermost stratosphere in summertime. The seasonal cycle of the CO variability in the troposphere is visible in the stratosphere up to 8 pvu. For PV greater than 8 pvu, the CO variability in the stratosphere is no longer in phase with the tropospheric cycle.

[39] For PV greater than 8 pvu, the normalized standard deviation of ozone (σ_{O3}) (Figure 5c) is at a maximum in the stratosphere between November and April, and at a minimum between May and September. This stratospheric variability is influenced by the Brewer-Dobson circulation which is at a maximum in wintertime and a minimum in summertime.

[40] We confirm here the results from *Krebsbach et al.* [2006] who also found a maximum of water vapor variability during summer and a maximum of ozone variability during spring in the lowermost stratosphere. A stronger impact of stratospheric air in the lowermost stratosphere is found in winter/spring and a greater impact of tropospheric air in summer/autumn [*Krebsbach et al.*, 2006; *Hegglin et al.*, 2006].

[41] In the troposphere, there is no evidence of a seasonal cycle of the ozone variability which is consistent with the previous study of *Logan* [1999a] at midlatitudes. The

maximum of ozone variability is observed between 2 and 4 pvu.

[42] The normalized standard deviations of ozone and CO show that the layer between 3 and 8 pvu is a transition layer between the chemical variability in the tropospheric and the stratospheric reservoirs.

[43] Figure 5e presents the monthly mean ozone/CO correlations. The most negative correlations occur between 4 and 6 pvu. Figure 5f shows the percentage of observations with an ozone/CO correlation less than -0.6, which is proportional to the percentage of observations where the mixing is governed by stirring. This percentage maximizes between 4 and 6 pvu (50%). Between 0 and 2 pvu, the ozone/CO correlations and the percentage of observations with the strongest anticorrelations are very low and have no seasonal variation. Between 2 to 4 pvu, these parameters are at a maximum in March and a minimum in August. This seasonal variation is probably due to a lower static stability near the tropopause during summertime (Figure 3). The diabatic mixing across isentropic surfaces (due to convective intrusions in the stratosphere) is more efficient and the timescale on which the signature of mixing governed by stirring remains visible becomes shorter. Between 6 and 8 pvu, the ozone/CO correlations and the percentage of observations with the strongest anticorrelations are at a maximum between July and September (-0.5 and 50%, respectively), and a minimum in February and April (-0.3 and 20%).

[44] Using the (α_o, PV_o) coordinate system and the ozone/CO correlations, we confirm for hundreds of flights the existence of a mixing layer above the tropopause where the mixing led by stirring is dominant. We have shown in this section the stratospheric and the tropospheric seasonal cycles of ozone and CO in the (α_o, PV_o) coordinate system. We also note that the strongest ozone/CO anticorrelations, denoting the existence of recent stirring in the mixing layer above the tropopause, correspond to the part of the coordinate system where the ozone and CO variabilities are related to a coupling between the tropospheric and stratospheric seasonal cycles of ozone and CO. On a PV surface, the strongest correlations are found for the largest α and the strongest wind speed, providing further evidence that the ozone and CO distributions in the mixing layer are dominated by the stirring from upper jet streams. Using an analysis with 1 pvu intervals (not shown), the mixing layer is located between 3 and 6 pvu in winter, spring and fall, and between 3 and 8 pvu between July and September. These results are in agreement with the results from *Hoor et al.* [2004] who have found a mixing layer with a thickness of 25 K between 2 and 6 pvu. They found a strong influence of stratospheric transport from the tropics to midlatitudes above the mixing layer, with a CO value of 35 ppbv representing the CO transported from the tropics. Below the mixing layer, convective mixing destroys the linear relationship between ozone and CO (up to 4 pvu during summertime). The ozone and CO distributions are mainly influenced by tropospheric chemistry and tropospheric transport. Above the mixing layer, diabatic processes and photochemistry reduce the relationship between ozone and CO. The ozone and CO distributions are mainly influenced by the stratospheric circulation [*Hoor et al.*, 2004] and stratospheric chemistry.

3.3. Lagrangian-Based Analysis

[45] Lagrangian-based studies have been used to analyze case studies of STE [*Hoor et al.*, 2002; *Pan et al.*, 2006] or to understand the seasonal and global variability of STE [*Sprenger and Wernli*, 2003; *James et al.*, 2003]. Using 15 years of ECMWF data, *Sprenger and Wernli* [2003] have studied stratosphere to troposphere transport (STT) and troposphere to stratosphere transport (TST). Concerning TST, they confirm the important role played by the polar and subtropical jet streams.

[46] We employ a Lagrangian technique to determine the origin of air parcels along the MOZAIC flight tracks, using back trajectories calculated with the LAGRANTO model [*Wernli and Davies*, 1997]. In this section we use different Lagrangian parameters to confirm the validity of the dynamic coordinate system and the results found in the previous section. We use a set of 5-day backward trajectories to study recent mixing.

[47] We used analyses of the European Centre for Medium-Range Weather Forecasts (ECMWF) available on 60 vertical levels from the surface up to 0.01 hPa for the description of the meteorological situation, analysis of the dynamical processes and calculation of backward trajectories. The 6-hourly analyses were supplemented with intermediate 3-hourly forecasts. Using 3-hourly wind fields with a good resolution (about 0.5° latitude-longitude) is essential for calculating trajectories as accurately as possible [*Stohl*, 1998]. However, the use of successive analysis and forecast for calculating trajectories can result in an overestimation of mixing along the trajectories [*Stohl et al.*, 2004]. A set of 5-day backward trajectories initialized along the flight tracks at 1-km intervals (approximately corresponding to the spatial resolution of the MOZAIC data) was calculated for each flight. To initialize backward trajectories at the exact location and time along the aircraft path, the wind fields were interpolated linearly in space and time using the two nearest ECMWF fields. This method assumes that the advection speed of features varies linearly in space and time.

[48] Figure 6 (top) presents three Lagrangian parameters in the dynamic coordinate system. The Lagrangian parameter τ_{st} represents the residence time in the stratosphere, calculated over 5 days, of the air masses having a tropospheric origin (PV $\leq$ 2 pvu) at the end point of the backward trajectory. The pyramid shape of τ_{st} in the dynamic coordinate system means that the greater the angle, the lower the depth of the ventilation (or longer). This pyramid shape is consistent with the fact that on a PV surface, the lowest potential temperatures are found in the center of the composite upper level trough, and thus, the tropospheric air masses are mixed deeper in the stratosphere at the center of the composite upper level trough than at the borders.

[49] The Lagrangian parameter STT represents the fraction of observations with PV greater than 6 pvu at the end of the 5-day back trajectories. This parameter represents the stratospheric transport from the stratosphere to the mixing layer. We use a threshold of 6 pvu since the upper limit of the mixing layer was defined by a value of 6 pvu in the previous section. The STT distribution is consistent with the observations in the previous section. The STT value is close to 100% for PV greater than 6 pvu, and close to 0 for PV

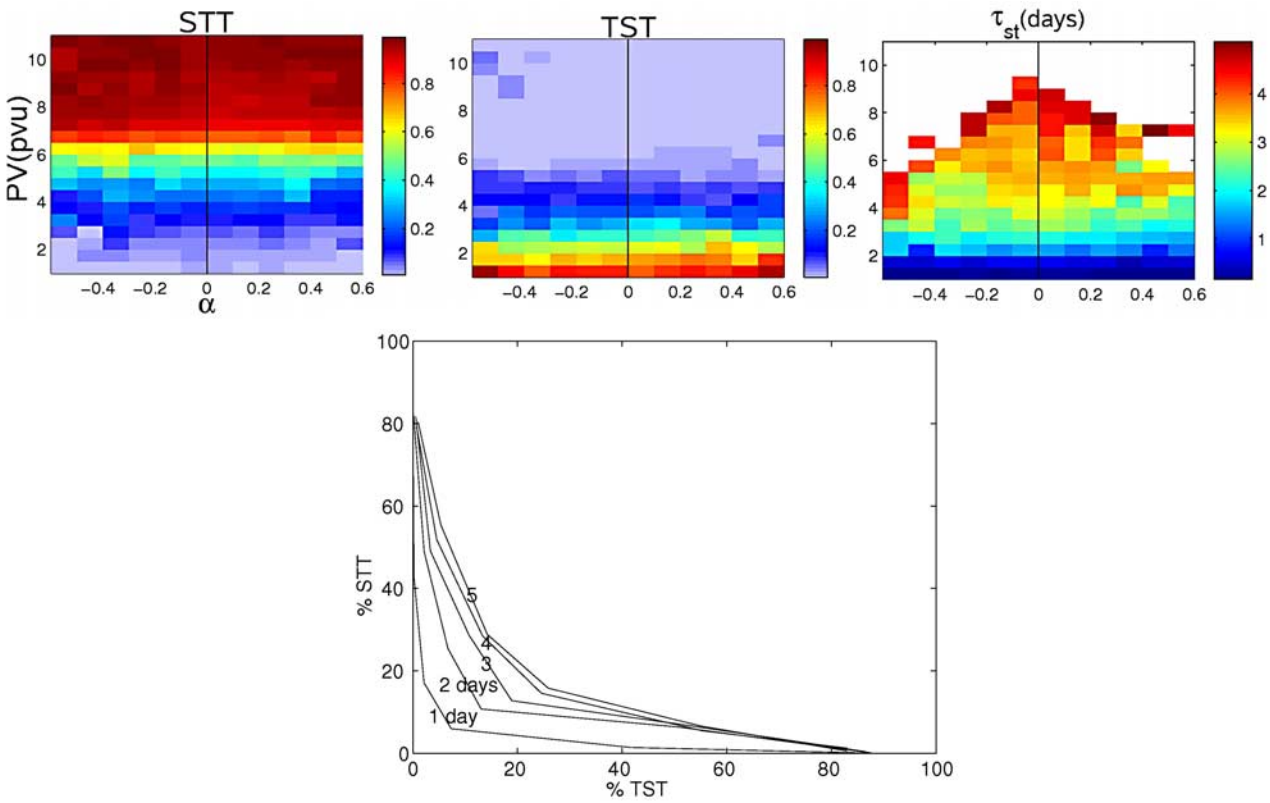

Figure 6. (top) Lagrangian parameters (left) STT, (middle) TST, and (right) τ_{st} (days) represent the percentage of stratospheric air masses (PV $\geq$ 6 pvu), tropospheric air masses (PV $\leq$ 2 pvu), and residence time of tropospheric air masses, respectively, over 5 days in the mixing layer in 2003. (bottom) Percentage of STT and TST in the center of the mixing layer (2 pvu $\leq$ PV $\leq$ 6 pvu, $-0.1 \leq \alpha \leq 0.1$) after 1, 2, 3, 4, and 5 days of backward transport.

values less than 2 pvu, defining the lower part of the mixing layer at about 2 pvu.

[50] The Lagrangian parameter TST represents the fraction of observations which have PV less than 2 pvu at the end of the 5-day backward trajectories, representing the tropospheric intrusions in the mixing layer. The TST parameter is significantly different from zero up to 6 pvu, confirming the location of the upper part of the mixing layer at about 6 pvu.

[51] The region where the STT and TST values are significantly higher than 0% and lower than 100% is associated with a region where mixing is relatively fast (less than 5 days) between the troposphere and the stratosphere. This region matches the same mixing layer found in the previous section where recent mixing governed by stirring is dominant.

[52] Figure 6 (bottom) presents the TST and STT parameters values found in the mixing layer after 1, 2, 3, 4 and 5 days of backward transport. As no convective or turbulent parameterizations are implemented in the LAGRANTO Lagrangian model, the STT and TST temporal evolution is mainly influenced by the resolved transport processes in the ECMWF fields, ie with a resolution no better than 0.5° in longitude/latitude. The temporal evolution of the STT and TST parameters, due to exchange between the troposphere the mixing layer and the stratosphere, is clearly reduced after 4 days. The intermingling between the mixing layer and the tropospheric and stratospheric reservoirs due to stirring is relatively fast as it can intermingle 80% of the mixing layer with the stratosphere and the troposphere at the upper and lower part of the mixing layer, and 40% at the center in 4 days. The stirring effect is probably the main process that drives stratospheric and tropospheric transport into the mixing layer over a time period of at least 4 days.

4. Regional Differences

[53] Figure 7 (left) presents the mean CO mixing ratios for each 1 pvu interval for the four seasons in 2003 and for 4 regions: North America (black, 100–20°W), North Atlantic (red, 60–20°W), Europe (green, 20°W–50°E) and Asia (blue, 60–140°E), for latitudes greater than 20°. For each PV value, a parametric analysis of variance test of the distributions of ozone and CO between the 4 regions has been applied. For each PV interval, the ozone and CO distribution between the 4 regions are significantly different at the 99% confidence interval. Thus, the following results based on the comparison of the CO and ozone means for the 4 different regions are relevant.

[54] Zonal variability of CO exists between these 4 regions. The seasonal cycle at 1 pvu over the North Atlantic and Europe is characterized by a maximum in winter and spring (110 ppbv) and a minimum in summer and fall

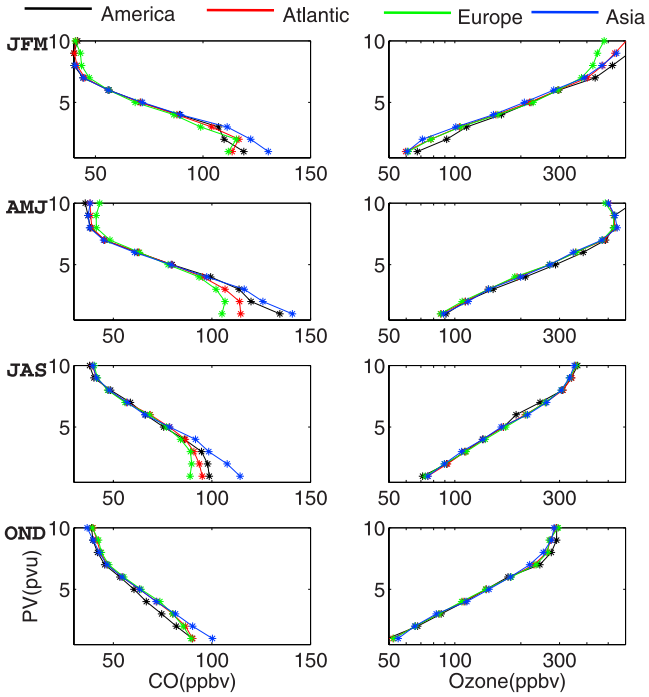

Figure 7. (left) Mean CO and (right) ozone mixing ratios for each 1 pvu interval, for the four time periods and four regions: North America, North Atlantic, Europe, and Asia. See the text for details on these regions.

(90 ppbv). Above North America, the maximum of CO occurs in spring (140 ppbv) and a minimum occurs in fall (90 ppbv). The Asia region is the most polluted during 2003. The maximum of CO occurs in spring (145 ppbv) and a minimum occurs in fall (100 ppbv). The maximum of CO over Asia between 1 and 3 pvu is the result of high anthropogenic surface emissions over Asia and from biomass burning over Russia which made a large contribution to the CO peaks over Asia in 2003 [e.g., *Nedelec et al.*, 2005].

[55] The tropospheric zonal variation influences the regional CO mixing ratios in the stratosphere up to 4 or 6 pvu, i.e., up to the upper part of the mixing layer, confirming the previous results that identified a tropospheric origin for the CO variability within the mixing layer. For PV values greater than 6 pvu, the 4 regions have the same PV/CO slope. This homogenization may be due to the fact that above 6 pvu, the mean residence time in the stratosphere is long enough that successive mixing undergone by the air masses does not allow the tropospheric chemical differences to be conserved.

[56] From winter to summer, the PV/CO slope is less negative between 1 and 4 pvu than between 4 and 6 pvu for certain regions. In spring and particularly in summer, the PV/CO slope is almost zero between 1 and 4 pvu over the North Atlantic and Europe. This zonal variation of the CO/PV gradient may be the consequence of recent mixing governed by stirring within the regional tropospheric air masses (with specific chemical signatures due to zonal and seasonal variability of surface sources) and the general stratospheric flow at 6 pvu which has the same chemical signature over the northern hemisphere. It is also possible that dynamical differences within the tropopause region may exist between these regions. These differences may come from the activity of the polar and subtropical jet streams in midlatitudes which may influence the efficiency of STE processes in each of these regions. Another possibility may come from differences of convection which are known to influence the chemical composition of the lowermost stratosphere [*Rosenlof et al.*, 1997], and may create turbulence zones which intensify the local mixing in the stratosphere and thus influence the CO/PV slope. Notice that the smallest slope is found in summer when deep convective intrusions are most efficient.

[57] Figure 7 (right) shows the mean ozone mixing ratios for each 1 pvu interval for the same time periods and regions as Figure 7 (left). There is no zonal variability of ozone for PV values less than 6 pvu.

[58] There are two likely reasons for the presence of a zonal CO gradient and the nonexistence of a zonal ozone gradient.

[59] 1. The ozone measurements are made near the tropopause region where the stratospheric ozone gradient is strong. A zonal gradient of ozone due to photochemical production differences in the troposphere might be difficult to identify because stratosphere-to-troposphere transport controls the ozone gradient in the tropopause region.

[60] 2. It is also possible that photochemical production of ozone occurs during the advection of the polluted plumes through the upper troposphere and the mixing zone. Therefore, the enhancement of ozone due to photochemical production does not necessarily match the region of high CO measurements and might be shifted zonally. For instance, ozone production from Asian emissions may be encountered over the western Pacific Ocean, far away from the MOZAIC aircraft pathways.

[61] Between 8 and 10 pvu, the ozone gradient is constant in spring, and has a zonal variability in winter, with a lower ozone mixing ratio over Europe. A constant ozone concentration during winter and spring has already been observed [*Logan*, 1999b; *Wang et al.*, 2006; *Randel et al.*, 2007], and is clearly visible 35 K above the tropopause [*Hegglin et al.*, 2006], and above 40 K for PV higher than 8 pvu [*Krebsbach et al.*, 2006]. *Randel et al.* [2007] have shown that the occurrence of low ozone in the lowermost stratosphere associated with double tropopause is significantly higher for cyclonic circulation in the UTLS (such as upper level troughs) than anticyclonic circulation. In spring, the CO concentration is also constant above the mixing layer with a mixing ratio of 40 ppbv indicating a tropical origin [*Hoor et al.*, 2004]. Several studies [*Bradshaw et al.*, 2002a, 2002b; *Lemoine*, 2004] have shown that Rossby waves can break in winter and spring near the subtropical jet, resulting in a poleward transport of tropical air into the extratropical lower stratosphere, resulting in air masses with low ozone and tropical CO mixing ratios above the mixing layer in midlatitudes. This process reduces the lower stratospheric ozone concentrations in winter and spring. This type of Rossby wave breaking occurs preferentially above the eastern Atlantic/Europe region, explaining why Europe is the region where the lowest ozone mixing ratios are observed in winter. The downward flux from the stratosphere to the lowermost stratosphere is greater in spring

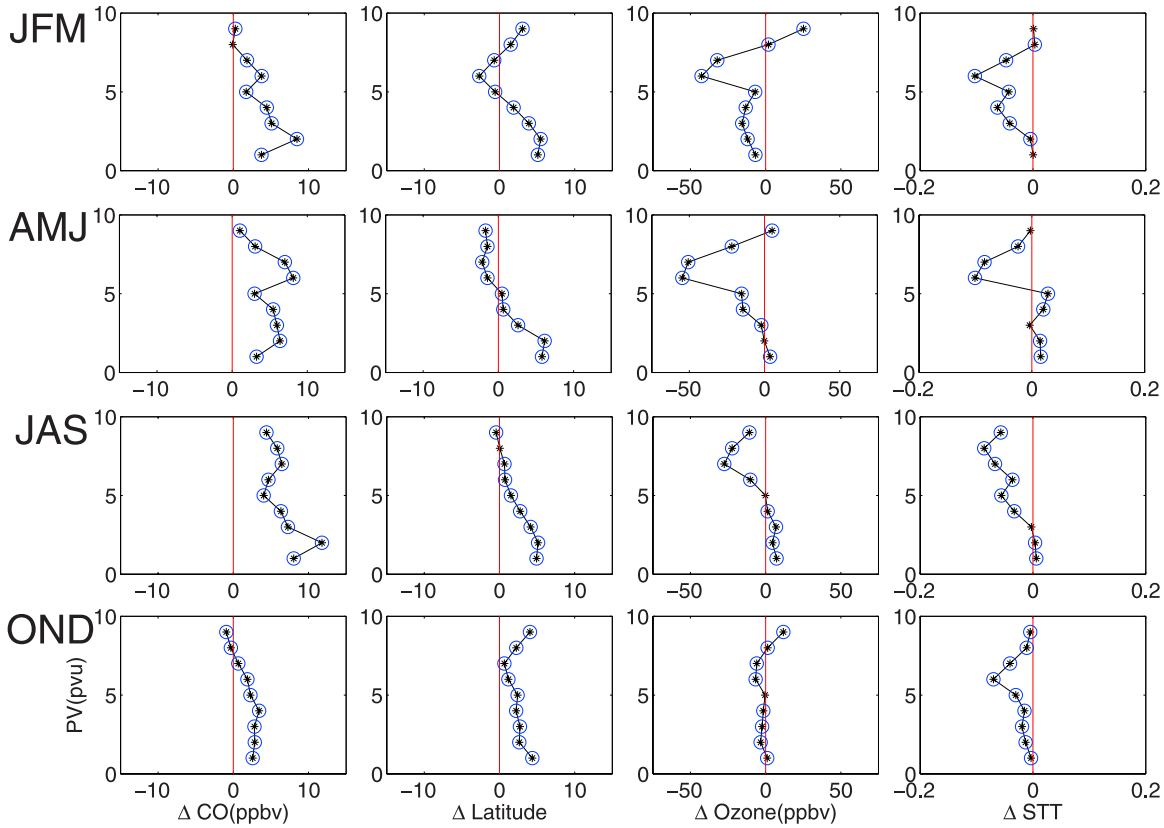

Figure 8. Differences of CO mixing ratio (ppbv) (first column), latitude (degrees) of each measurement after 5 days of backward transport (second column), ozone mixing ratio (ppbv) (third column), and STT Lagrangian parameter (fraction) (fourth column) computed by substracting the values at the center from the values at the borders, for the four seasons in 2003. A positive difference signifies a higher value at the center. The circles indicate the PV ranges where the distributions between the center and the borders are significantly different at the 99% confidence interval. See the text for details.

[*Appenzeller et al.*, 1996], and is probably the reason why the zonal variability of ozone is lower in spring than in winter. The region above the jet stream can be turbulent because of gravity waves generated by the jet streams [*Pavelin et al.*, 2001; *Pavelin and Whiteway*, 2002; *Koch et al.*, 2005], which may be responsible for the absence of a gradient in ozone and CO above the mixing layer in winter and spring (PV $\geq$ 8 pvu).

5. Differences Between the Center and the Borders of Upper Level Troughs

[62] In this section we examine the differences of the ozone and CO distributions between the center and the borders of upper level troughs. we define the center of composite upper level troughs with $|\alpha| \leq 0.05$ and the borders with $|\alpha| \geq 0.15$. The results in this section are not sensitive to the thresholds used to define the center and borders.

[63] Figure 8 shows the differences between the center and the borders by substracting the mean CO mixing ratio (ppbv) at the center from the CO mixing ratio at the borders (first column). Similarly, the differences in latitude for each 1 pvu interval that had MOZAIC measurements after 5 days of backward trajectories (second column), the differences of ozone(ppbv) (third column), and STT (fourth column) are also depicted. A positive value means that the parameter is greater at the center than at the border, and vice versa. The conclusions found in this section based on the absolute differences in ozone and CO (in ppbv) are also valid for the relative differences in ozone and CO (%). For each PV value, a parametric analysis of variance of ozone and CO between the center and the borders has been applied. For each PV interval, the circles in Figure 8 indicate the PV intervals where the distributions are significantly different at the 99% confidence interval. We discuss in this section the most significant differences.

[64] The ozone mixing ratios (Figure 8, third column) at the borders are higher than at the center (negative values) between 6 and 8 pvu in winter (−40 ppbv), spring (−55 ppbv) and summer (−27 ppbv). For PV values lower or higher, there is no significant ozone difference. These chemical differences are only observed at the upper part of the mixing layer. STT (Figure 8, fourth column) follows the same behavior as the ozone, with significant negative differences (up to 10%) observed between 4 and 8 pvu. In fall, the differences are less than 6%.

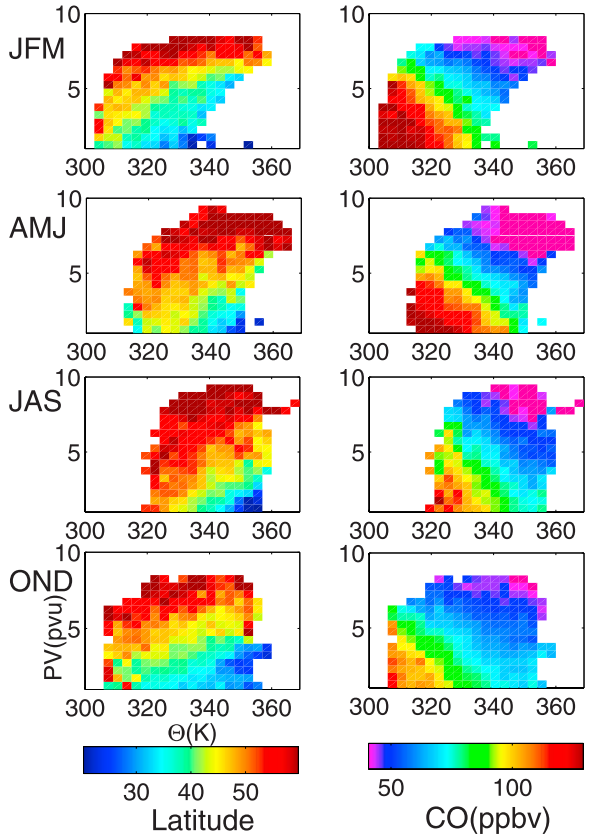

Figure 9. (right) Mean CO (ppbv) and (left) latitude (degrees) after 5 days of backward transport averaged in θ and PV grid cells for the four seasons in 2003.

[65] The CO mixing ratio (Figure 8, first column) at the center is greater than at the borders (positive values), throughout the mixing layer, with a relative minimum at 5 pvu, in winter, spring and summer. The relative maximum of CO for PV higher than 5 pvu can be explained by the previous explanations regarding the ozone differences. The stratospheric transport into the mixing layer is stronger at the borders than at the center. This process preferentially advects air masses with lower CO mixing ratios to the borders than to the center, explaining the greater CO mixing ratios at the center above 5 pvu.

[66] The θ field in the (α_o, PV_o) coordinate system of Figure 4 shows that the high ozone, high STT and low CO at the edges are associated with high θ, while the low ozone, low STT and high CO at the center are associated with low θ. This indicates that there is a greater transport of tropospheric air into the center of the trough between 6 and 8 pvu than into the edges, particularly in spring. While the edges of the trough are closer to the troposphere in a spatial sense, the greater θ values make it more difficult for tropospheric air masses (and in particular those from the surface) to be transported into these regions of the trough. The center of the trough however has lower θ values making it, from the thermodynamic point of view, closer to the surface emissions. We speculate that a possible transport mechanism is the same process that causes wrap around moisture to penetrate into the center of an upper trough when a midlatitude cyclone reaches a mature phase. *Cooper et al.* [2001] has demonstrated such a transport mechanism for a polluted air parcel in the upper troposphere, just below the stratosphere. These differences of ozone and CO between the borders and the center are not visible for PV values lower than 4 pvu because at the lower part of the mixing layer, the θ values are small enough at both the center and at the borders to allow quasi-horizontal transport and mixing across the tropopause in the whole upper level trough, which reduces the ozone, STT and CO differences between the center and the borders.

[67] The relative maximum of CO at the center for PV less than 5 pvu can be explained by the θ field in the (α_o, PV_o) coordinate system on Figure 4 (second row) that shows isentropic surfaces have lower θ at the center than at the borders. Figure 8 (second column) shows the differences of latitude between the center and the borders for each 1 pvu interval that had MOZAIC measurements after 5 days of backward trajectories. The air masses at the center originated from higher latitudes for PV lower than 5 pvu. Figure 9 presents the mean CO and mean latitude after 5 days of backward trajectories in each grid cell of PV and potential temperature (θ), for the four seasons in 2003. For a given PV surface, the higher the θ value, the lower the CO mixing ratio and the lower the latitude. It confirms the existence of a meridional gradient of CO in the upper troposphere.

[68] As a consequence, in the lower part of the mixing layer, the air masses on the borders of the upper level troughs predominantly originated within the subtropics where the mean CO mixing ratio is lower than at midlatitudes. The air masses at the center of the upper level troughs originate mainly in midlatitudes and have more CO.

6. Differences Between the East and West Sides of Upper Level Troughs

[69] In the presence of a cold front at the surface, the east side of an upper level trough is associated with a warm conveyor belt, considered as the main transport mechanism from the boundary layer to the upper troposphere in midlatitudes [*Stohl*, 2001; *Cooper et al.*, 2001; *Esler et al.*, 2003] and is important for the transport of polluted air masses [*Stohl and Trickl*, 1999; *Cooper et al.*, 2002a, 2002b; *Eckhardt et al.*, 2004]. The dry airstream (DA) is a coherent airstream that descends isentropically from the tropopause region on the west side of the trough into the middle and lower troposphere toward the center of the maturing cyclone, and transports dry and possibly stratospheric origin air masses [*Wernli*, 1997; *Cooper et al.*, 1998; *Stohl and Trickl*, 1999]. The irreversible transport from the stratosphere to the troposphere is related to fine-scale structures like tropopause folds and filaments [*Danielsen*, 1968; *Shapiro*, 1978; *Vaughan et al.*, 1994; *Appenzeller et al.*, 1996].

[70] In this section we examine the difference of ozone and CO mixing ratios between the east and west sides of upper level troughs. We define the east side of the synthetic upper troughs with $|\alpha| \geq 0.15$ and the west side with $|\alpha| \leq -0.15$. The results in this section are not sensitive to the thresholds used to define the east and west sides. The conclusions found in this section based on the absolute

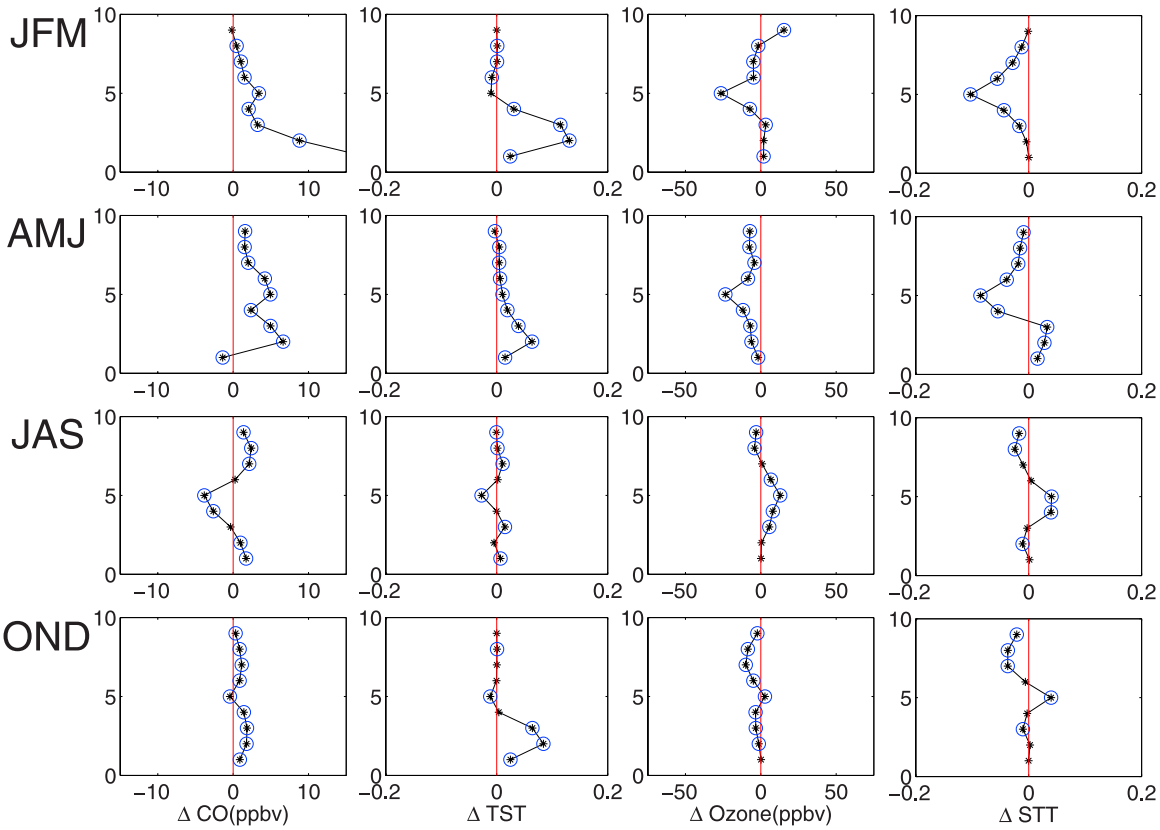

Figure 10. Differences of CO mixing ratio (ppbv) (first column), TST Lagrangian parameter (fraction) (second column), ozone mixing ratio (ppbv) (third column), and STT Lagrangian parameter (fraction) (fourth column) computed by substracting the values on the east side from the values on the west side, for the four seasons in 2003. A positive difference signifies that the value is higher on the east side. The circles indicate the PV ranges where the distributions between the center and the borders are significantly different at the 99% confidence interval. See the text for details.

differences in ozone and CO (in ppbv) are also valid for the relative differences in ozone and CO (%).

[71] Figure 10 shows the differences of CO mixing ratios by substracting the mean CO mixing ratio (ppbv) at the east side from the CO mixing ratio at the west side (first column). Similarly, the differences of TST (second column), the differences of ozone(ppbv) (third column), and STT (fourth column) are also depicted. A positive value means that the parameter is higher at the east side than at the west side, and vice versa. For each PV value, a parametric analysis of variance of ozone and CO between the east and the west side has been applied. For each PV interval, the circles in Figure 10 indicate the PV intervals where the distributions are significantly different at the 99% confidence interval. We discuss in this section the most significant differences.

[72] The ozone mixing ratio and STT is greater on the west side than on the east side (negative value) at about 5 pvu in winter (−26 ppbv and −10%) and spring (−24 ppbv and −9%). At 5 pvu, the CO mixing ratio is higher on the east side than on the west (positive value, +5 ppbv) in spring.

[73] In summer, the ozone mixing ratio and STT is higher (+13 ppbv and +4%) on the east side than on the west side, while the CO mixing ratio is higher on the west than on the east side (−4 ppbv). No significant difference in ozone and CO is found during fall season.

[74] Within the lower part of the mixing layer, no significant ozone difference is found. However, the CO mixing ratio and TST are higher on the east side than on the west side in winter (+17.5 ppbv and +13%) and spring (+7 ppbv and +6%). No CO difference is found in summer and fall.

[75] Within the upper part of the mixing layer, the ozone and CO differences, correlated with STT, seem to be the consequence of stronger stratosphere to mixing layer transport on the west side than on the east in winter and spring. This transport is stronger on the east side than on the west side during summer. Within the lower part of the mixing layer, the CO mixing ratio and TST is higher on the east side than on the west side, in winter and spring. A stronger troposphere to mixing layer transport on the east side than on the west side in winter and spring is probably responsible for this CO difference.

[76] The ozone and CO differences between the east side and the west side seem to be the consequence of a predominantly troposphere to mixing layer transport on the east side, and a predominantly stratosphere to mixing layer transport on the west side, which is consistent with previous studies. These differences are fairly small com-

pared to the differences found between the center and the borders of upper level troughs, and further study is required to more fully understand the dynamic processes and their variation between winter and summer.

7. Conclusions

[77] MOZAIC ozone and CO measurements from 2003 were mapped into a new dynamic coordinate system which provides a coherent view of observations within upper level troughs. The coordinate system is based on the angle α between the local PV surfaces and the horizontal on the x axis, and PV on the y axis. This coordinate system allows the study of the zonal and seasonal variations of the chemical composition of the tropopause region in midlatitude baroclinic waves and allows the identification of the mixing layer near the tropopause. We have focused our study on upper level troughs because the MOZAIC flights have more extensive vertical sampling across upper level troughs than ridges. The behavior of wind speed, potential temperature, and relative vorticity in the (α_o, PV_o) coordinate system confirms the validity of the method.

[78] Using the (α_o, PV_o) coordinate system, we establish for the first time the ozone and CO distribution in a composite upper level trough and identify (1) the seasonal cycle of stratospheric and tropospheric ozone and CO mixing ratios in the upper troposphere and lowermost stratosphere within upper level troughs; (2) a mixing layer in the tropopause region of upper level troughs, where zonal differences are characterized and where ozone and CO anomalies are encountered in the center and along the borders, and between the east and west sides of upper level troughs; and (3) seasonal cycles of these chemical anomalies.

[79] The seasonal cycles of ozone and CO in the upper troposphere and the lower stratosphere have been investigated. The tropospheric ozone cycle has a maximum in May–June (83 ppbv) and a minimum in November to January (47 ppbv). The stratospheric ozone cycle has a maximum in April (640 ppbv) and a minimum in October (265 ppbv). The seasonal cycle of CO has a maximum in the upper troposphere in April–May (125 ppbv) and a minimum in September–November (91 ppbv). The stratospheric CO (above 7 pvu) has a minimum in April (37 ppbv) and a maximum in August (45 ppbv).

[80] A mixing layer in the tropopause region was identified between 2 and 6 pvu and up to 8 pvu in summer. The strongest ozone/CO anticorrelations calculated over 50 km are observed in this mixing layer, and particularly near the strongest wind speed, confirming the hypothesis that the main process which redistributes ozone and CO in the tropopause region is the stirring effect generated by upper level jet streams. The seasonal cycle of ozone and CO inside this mixing layer is a combination of both the tropospheric and stratospheric seasonal cycles. Diabatic processes from convective transport probably dominate the ozone and CO distribution at the lower part of the mixing layer (between 2 and 3 pvu), particularly during summertime (up to 4 pvu).

[81] Regional differences in the mixing layer have been observed between 2 and 4 pvu, and up to 6 pvu in summertime. Asia is the most polluted region especially in spring (140 ppbv) because of high CO surface emissions from biomass burning in the north and anthropogenic pollution in the south.

[82] A Lagrangian-based analysis was applied to each MOZAIC measurement and placed in the dynamic coordinate system. We estimate that large-scale transport, probably the stirring effect from upper level jet streams, can mix 40% of the mixing layer with the tropospheric and stratospheric reservoirs at the center and 80% at the edges over a time period of 4 days. The stirring effect is probably the main process that governs the chemical composition of the mixing layer over at least 4 days. We still need to improve our Lagrangian study by using a Lagrangian model with convective and turbulent schemes.

[83] These Lagrangian parameters were also used to explain the chemical differences in ozone and CO found between the center and the borders of upper level troughs. Within the upper part of the mixing layer, the ozone mixing ratios are greater at the borders than at the center, while the CO mixing ratios are greater at the center than at the borders. This is due to the fact that troposphere to mixing layer transport occur preferentially at the center. A seasonal cycle of ozone and CO differences is found, with a maximum in winter and spring, and minimum in fall. Within the lower part of the mixing layer, the CO mixing ratio is greater at the center than at the borders. This is due to the fact that air masses at the borders of the mixing layer come preferentially from the subtropics while the air masses at the center of the mixing layer come preferentially from the midlatitudes. Furthermore, the Lagrangian analysis and the CO measurements from MOZAIC show a meridional gradient of CO from the subtropics to the midlatitudes which explains this positive anomaly in the mixing layer.

[84] Chemical differences have also been found between the east and west sides of upper level troughs. Within the upper part of the mixing layer, the stratosphere to mixing layer transport occurs preferentially on the west side of the synthetic upper level trough, especially in winter and spring, related to greater ozone mixing ratios on the west side, and greater CO mixing ratios on the east side. Within the lower part of the mixing layer, the troposphere to mixing layer transport occur preferentially on the east side, which enhances the CO mixing ratio on the east side.

[85] We have shown the usefulness of this technique and the link between STE and the spatial distribution of ozone and CO in a composite upper level trough. However, in future work the use of the FLEXPART Lagrangian dispersion model will increase the accuracy of the Lagrangian study in the mixing layer by calculating the turbulent transport in the stratosphere. Its convection scheme will allow us to study large tropospheric intrusions into the mixing layer. Furthermore, the use of the (α_o, PV_o) coordinate system to study ozone and CO distributions with chemical transport models will allow us to assess the representation of STE processes in these models by comparing their results with the chemical distributions found with in situ measurements from MOZAIC aircraft.

[86] **Acknowledgments.** The authors would like to thank the reviewers for their helpful and constructive suggestions and comments. Thanks are also due to Olivier Pujol for his useful discussions. The authors acknowledge the strong support of the European Communities, EADS, Airbus, and the airlines (Lufthansa, Austrian, and Air France) who carry

free of charge the MOZAIC equipment and perform the maintenance since 1994.

References

Allen, D. R., and N. Nakamura (2003), Tracer equivalent latitude: A diagnostic tool for isentropic transport studies, *J. Atmos. Sci.*, *60*(2), 287–304.

Appenzeller, C., J. R. Holton, and K. H. Rosenlof (1996), Seasonal variation of mass transport across the tropopause, *J. Geophys. Res.*, *101*(D10), 15,071–15,078.

Bell, G. D., and D. Keyser (1993), Shear and curvature vorticity and potential vorticity interchanges—Interpretation and application to a cutoff cyclone event, *Mon. Weather Rev.*, *121*(1), 76–102.

Bradshaw, N., G. Vaughan, and G. Ancellet (2002a), Generation of layering in the lower stratosphere by a breaking Rossby wave, *J. Geophys. Res.*, *107*(D2), 4011, doi:10.1029/2001JD000432.

Bradshaw, N. G., G. Vaughan, R. Busen, S. Garcelon, R. Jones, T. Gardiner, and J. Hacker (2002b), Tracer filamentation generated by small-scale Rossby wave breaking in the lower stratosphere, *J. Geophys. Res.*, *107*(D23), 4689, doi:10.1029/2002JD002086.

Cooper, O. R., J. L. Moody, J. C. Davenport, S. J. Oltmans, B. J. Johnson, X. Chen, P. B. Shepson, and J. T. Merrill (1998), Influence of springtime weather systems on vertical ozone distributions over three North American sites, *J. Geophys. Res.*, *103*(D17), 22,001–22,013.

Cooper, O. R., J. L. Moody, D. D. Parrish, M. Trainer, T. B. Ryerson, J. S. Holloway, G. Hubler, F. C. Fehsenfeld, S. J. Oltmans, and M. J. Evans (2001), Trace gas signatures of the airstreams within North Atlantic cyclones: Case studies from the North Atlantic Regional Experiment (NARE-97) aircraft intensive, *J. Geophys. Res.*, *106*(D6), 5437–5456.

Cooper, O. R., J. L. Moody, D. D. Parrish, M. Trainer, T. B. Ryerson, J. S. Holloway, G. Hubler, F. C. Fehsenfeld, and M. J. Evans (2002a), Trace gas composition of midlatitude cyclones over the western North Atlantic Ocean: A conceptual model, *J. Geophys. Res.*, *107*(D7), 4056, doi:10.1029/2001JD000901.

Cooper, O. R., J. L. Moody, D. D. Parrish, M. Trainer, J. S. Holloway, G. Hubler, F. C. Fehsenfeld, and A. Stohl (2002b), Trace gas composition of midlatitude cyclones over the western North Atlantic Ocean: A seasonal comparison of ozone and CO, *J. Geophys. Res.*, *107*(D7), 4057, doi:10.1029/2001JD000902.

Crutzen, P., M. Lawrence, and U. Pöschl (1999), On the background photochemistry of tropospheric ozone, *Tellus*, *51*, 123–146.

Danielsen, E. F. (1968), Stratospheric-tropospheric exchange based upon radioactivity, ozone and potential vorticity, *J. Atmos. Sci.*, *25*, 502–518.

Eckhardt, S., A. Stohl, H. Wernli, P. James, C. Forster, and N. Spichtinger (2004), A 15-year climatology of warm conveyor belts, *J. Clim.*, *17*, 218–237.

Esler, J. G., P. H. Haynes, K. S. Law, H. Barjat, K. Dewey, J. Kent, S. Schmitgen, and N. Brough (2003), Transport and mixing between air masses in cold frontal regions during Dynamics and Chemistry of Front Zones (DCFZ), *J. Geophys. Res.*, *108*(D4), 4142, doi:10.1029/2001JD001494.

Forster, P. M. D., and K. P. Shine (1997), Radiative forcing and temperature trends from stratospheric ozone changes, *J. Geophys. Res.*, *102*, 10,841–10,855.

Grewe, V. (2006), The origin of ozone, *Atmos. Chem. Phys.*, *6*, 1495–1511.

Hauglustaine, D. A., G. R. Brasseur, S. Walters, P. J. Rasch, J.-F. Müller, L. K. Emmons, and M. A. Carroll (1998), MOZART, a global chemical transport model for ozone and related chemical tracers: 2. Model results and evaluation, *J. Geophys. Res.*, *103*(D21), 28,291–28,335.

Haynes, P. H., and J. Anglade (1997), The vertical-scale cascade in atmospheric tracers due to large-scale differential advection, *J. Atmos. Sci.*, *54*, 1121–1136.

Hegglin, M. I., et al. (2006), Measurements of NO, NO_y, N_2O and ozone during SPURT: Implications for transport and chemistry in the lowermost stratosphere, *Atmos. Chem. Phys.*, *6*, 1331–1350.

Hoor, P., H. Fischer, L. Lange, J. Lelieveld, and D. Brunner (2002), Seasonal variations of a mixing layer in the lowermost stratosphere as identified by the CO-O_3 correlation from in situ measurements, *J. Geophys. Res.*, *107*(D5), 4044, doi:10.1029/2000JD000289.

Hoor, P., C. Gurk, D. Brunner, M. I. Hegglin, H. Wernli, and H. Fischer (2004), Seasonality and extent of extratropical TST derived from in-situ CO measurements during SPURT, *Atmos. Chem. Phys.*, *4*, 1427–1442.

Hoor, P., H. Fischer, and J. Lelieveld (2005), Tropical and extratropical tropospheric air in the lowermost stratosphere over Europe: A CO-based budget, *Geophys. Res. Lett.*, *32*, L07802, doi:10.1029/2004GL022018.

Hoskins, B. J., M. E. McIntyre, and A. W. Robertson (1985), On the use and significance of isentropic potential vorticity maps, *Q. J. R. Meteorol. Soc.*, *111*, 877–946.

Intergovernmental Panel on Climate Change (2001), *Climate Change 2001: The Scientific Basis—Contribution of Working Group 1 to the Third Assessment Report of the Intergovernmental Panel on Climate Change*, edited by J. T. Houghton et al., Cambridge Univ. Press, New York.

James, P., A. Stohl, C. Forster, S. Eckhardt, P. Seibert, and A. Frank (2003), A 15-year climatology of stratosphere-troposphere exchange with a Lagrangian particle dispersion model: 2. Mean climate and seasonal variability, *J. Geophys. Res.*, *108*(D12), 8522, doi:10.1029/2002JD002639.

Koch, S. E., B. D. Jamison, C. Lu, T. L. Smith, E. I. Tollerud, N. Wang, T. P. Lane, M. A. Shapiro, D. D. Parrish, and O. R. Cooper (2005), Turbulence and gravity waves within an upper-level front, *J. Atmos. Sci.*, *62*(11), 3885–3908, doi:10.1175/JAS3574.1.

Krebsbach, M., et al. (2006), Seasonal cycles and variability of ozone and H_2O in the UT/LMS during SPURT, *Atmos. Chem. Phys.*, *6*, 109–125.

Lary, D. J., et al. (1995), Three dimensional tracer initialization and general diagnostics using equivalent PV latitude potential temperature coordinates, *Q. J. R. Meteorol. Soc.*, *121*, 187–210.

Lemoine, R. (2004), Secondary maxima in ozone profiles, *Atmos. Chem. Phys.*, *4*, 1085–1096.

Logan, J. A. (1999a), An analysis of ozonesonde data for the troposphere: Recommendations for testing 3-D models and development of a gridded climatology for tropospheric ozone, *J. Geophys. Res.*, *104*(D13), 16,115–16,150, doi:10.1029/1998JD100096.

Logan, J. A. (1999b), An analysis of ozonesonde data for the lower stratosphere: Recommendations for testing models, *J. Geophys. Res.*, *104*(D13), 16,151–16,170, doi:10.1029/1999JD900216.

Manney, G. L., et al. (1999), Polar vortex dynamics during spring and fall diagnosed using trace gas observations from the atmospheric trace molecul spectroscopy instrument, *J. Geophys. Res.*, *104*, 19,243–19,255.

Marenco, A., et al. (1998), Measurement of ozone and water vapor by Airbus in-service aircraft: The MOZAIC airborne program, An overview, *J. Geophys. Res.*, *103*(D19), 25,631–25,642.

Nédélec, P., J.-P. Cammas, V. Thouret, G. Athier, J.-M. Cousin, C. Legrand, C. Abonnel, F. Lecoeur, G. Cayez, and C. Marizy (2003), An improved infrared carbon monoxide analyser for routine measurements aboard commercial Airbus aircraft: Technical validation and first scientific results of the MOZAIC III programme, *Atmos. Chem. Phys.*, *3*, 1551–1564.

Nedelec, P., V. Thouret, J. Brioude, B. Sauvage, J.-P. Cammas, and A. Stohl (2005), Extreme CO concentrations in the upper troposphere over northeast Asia in June 2003 from the in situ MOZAIC aircraft data, *Geophys. Res. Lett.*, *32*, L14807, doi:10.1029/2005GL023141.

Novelli, P. C., K. A. Masarie, and P. M. Lang (1998), Distribution and recent changes in atmospheric carbon monoxide, *J. Geophys. Res.*, *103*, 19,015–19,033.

Pan, L. L., W. J. Randel, B. L. Gary, M. J. Mahoney, and E. J. Hintsa (2004), Definitions and sharpness of the extratropical tropopause: A trace gas perspective, *J. Geophys. Res.*, *109*, D23103, doi:10.1029/2004JD004982.

Pan, L. L., P. Konopka, and E. V. Browell (2006), Observations and model simulations of mixing near the extratropical tropopause, *J. Geophys. Res.*, *111*, D05106, doi:10.1029/2005JD006480.

Pavelin, E., and J. A. Whiteway (2002), Gravity wave interactions around the jet stream, *Geophys. Res. Lett.*, *29*(21), 2024, doi:10.1029/2002GL015783.

Pavelin, E., J. A. Whiteway, and G. Vaughan (2001), Observation of gravity wave generation and breaking in the lowermost stratosphere, *J. Geophys. Res.*, *106*(D6), 5173–5180, doi:10.1029/2000JD900480.

Polvani, L. M., and J. G. Esler (2007), Transport and mixing of chemical air masses in idealized baroclinic life cycles, *J. Geophys. Res.*, *112*, D23102, doi:10.1029/2007JD008555.

Randel, W. J., D. J. Seidel, and L. L. Pan (2007), Observational characteristics of double tropopauses, *J. Geophys. Res.*, *112*, D07309, doi:10.1029/2006JD007904.

Ray, E. A., et al. (1999), Transport into the Northern Hemisphere lowermost stratosphere revealed by in situ tracer measurements, *J. Geophys. Res.*, *104*(D21), 26,565–26,580, doi:10.1029/1999JD900323.

Rosenlof, K. H., A. F. Tuck, K. K. Kelly, J. M. Russell, and M. P. McCormick (1997), Hemispheric asymmetries in water vapor and inferences about transport in the lower stratosphere, *J. Geophys. Res.*, *102*(D11), 13,213–13,234.

Seo, K. H., and K. P. Bowman (2001), A climatology of isentropic cross-tropopause exchange, *J. Geophys. Res.*, *106*, 28,159–28,172.

Shapiro, M. A. (1978), Further evidence of the mesoscale and turbulent structure of upper level jet stream-frontal zone systems, *Mon. Weather Rev.*, *106*, 1100–1111.

Sprenger, M., and H. Wernli (2003), A northern hemispheric climatology of cross-tropopause exchange for the ERA15 time period (1979–1993), *J. Geophys. Res.*, *108*(D12), 8521, doi:10.1029/2002JD002636.

Stevenson, D. S., et al. (2006), Multimodel ensemble simulations of present-day and near-future tropospheric ozone, *J. Geophys. Res.*, *111*, D08301, doi:10.1029/2005JD006338.

Stohl, A. (1998), Computation, accuracy and application of trajectories—A review and bibliography, *Atmos. Environ.*, *32*, 947–966.

Stohl, A. (2001), A 1-year Lagrangian "climatology" of airstreams in the Northern Hemisphere troposphere and lowermost stratosphere, *J. Geophys. Res.*, *106*(D7), 7263–7279.

Stohl, A., and T. Trickl (1999), A textbook example of long-range transport: Simultaneous observations of ozone maxima of stratospheric and North American origin in the free troposphere over Europe, *J. Geophys. Res.*, *104*(30), 445–462.

Stohl, A., S. Eckhardt, C. Forster, P. James, and N. Spichtinger (2002), On the pathways and timescales of intercontinental air pollution transport, *J. Geophys. Res.*, *107*(D23), 4684, doi:10.1029/2001JD001396.

Stohl, A., et al. (2003), Stratosphere-troposphere exchange: A review, and what we have learned from STACCATO, *J. Geophys. Res.*, *108*(D12), 8516, doi:10.1029/2002JD002490.

Stohl, A., O. R. Cooper, and P. James (2004), A cautionary note on the use of meteorological analysis fields for quantifying atmospheric mixing, *J. Atmos. Sci.*, *61*, 1446–1453.

Thouret, V., A. Marenco, P. Nédélec, and C. Grouhel (1998a), Ozone climatologies at 9–12 km altitude as seen by the MOZAIC airborne program between September 1994 and August 1996, *J. Geophys. Res.*, *103*, 25,653–25,679.

Thouret, V., A. Marenco, J. Logan, P. Nédélec, and C. Grouhel (1998b), Comparisons of ozone measurements from the MOZAIC airborne program and the ozone sounding network at eight locations, *J. Geophys. Res.*, *103*, 25,695–25,720.

Vaughan, G., J. D. Price, and A. Howells (1994), Transport into the troposphere in a tropopause fold, *Q. J. R. Meteorol. Soc.*, *120*, 1085–1103.

Wang, P.-H., D. M. Cunnold, C. R. Trepte, H. J. Wang, P. Jing, J. Fishman, V. G. Brackett, J. M. Zawodney, and G. E. Bodeker (2006), Ozone variability in the midlatitude upper troposphere and lower stratosphere diagnosed from a monthly SAGE II climatology relative to the tropopause, *J. Geophys. Res.*, *111*, D21304, doi:10.1029/2005JD006108.

Wernli, H. (1997), A Lagrangian-based analysis of extratropical cyclones. II: A detailed case study, *Q. J. R. Meteorol. Soc.*, *123*, 1677–1706.

Wernli, H., and H. C. Davies (1997), A Lagrangian-based analysis of extratropical cyclones. I: The method and some applications, *Q. J. R. Meteorol. Soc.*, *123*, 467–489.

J. Brioude and O. Cooper, Chemical Sciences Division, Earth System Research Laboratory, NOAA, Boulder, CO 80305, USA. (jerome.brioude@noaa.gov)

J.-P. Cammas and P. Nedelec, Laboratoire d'Aérologie, UMR5560, CNRS, Observatoire Midi-Pyrénées, F-31400 Toulouse, France.